Electrical Power and Energy Systems 172 (2025) 111301

Contents lists available at ScienceDirect

International Journal of Electrical Power and Energy Systems

journal homepage: www.elsevier.com/locate/ijepes

Where stability meets efficiency: A practical preventive control strategy for Microgrids

Giulia Amato *, Luigi Pio Savastio, Enrico Elio De Tuglie

Department of Electrical and Information Engineering, Politecnico di Bari, Bari, Italy

ARTICLE INFO

Keywords:
Feasibility region
Convex hull
Microgrid
Practical stability
Preventive control strategy
Security

ABSTRACT

The energy transition, while undeniably offering countless advantages, has increasingly subjected electrical systems to stress conditions that may jeopardize their secure operation. To address this challenge, a wide range of control strategies has been developed. This work proposes a proactive and computationally efficient methodology, specifically designed to align with the capabilities of a smart MicroGrid (μG). The approach leverages the offline characterization of a feasibility region, defined as a convex structure in the operational space of the electrical system, to ensure secure operation within time frames compatible with real-time management for such a constrained system. The proposed method evaluates the stability and security of an operating point derived from an economic dispatch. When this point fails to meet predefined security requirements, the methodology identifies an alternative operating condition that ensures system security while minimizing deviations from the economically optimal state. The effectiveness of this approach has been validated through a case study replicating a subset of the experimental μG implemented in the PrInCE Lab at Polytechnic University of Bari.

1. Introduction

How many times have we witnessed, either directly or through the media, the increasingly evident effects of climate change on our planet? The last decade has been the warmest on record, as highlighted by the World Meteorological Organization [1]. The consequences, already extensively documented, profoundly impact ecosystems and human quality of life, demanding immediate global action.

In response to this crisis, the energy transition has emerged as a global priority. The adoption of sustainable policies and the integration of Renewable Energy Sources (RES) aim to reduce reliance on fossil fuels. However, the shift toward a non programmable RES-based energy system introduces significant challenges, such as reduced system inertia in power grids that are already under increasing stress due to the increase in energy demand [2–4]. This phenomenon affects the stability, quality and resilience of electrical networks [5–7].

Distributed Energy Resources (DER) and smart MicroGrids (μG), which combine DER with advanced energy management techniques, offer promising solutions. Scientific studies [8,9] highlight how μG systems reduce dependency on the main grid and promote active consumer participation. Additionally, they facilitate the transition to a decentralized and resilient energy model [10,11]. To fully exploit the potential of DER and μG systems, it is essential to address the challenges related to the low inertia of power electronic devices, which DERs are usually equipped with, which can make the systems vulnerable to disturbances and lead to blackouts. Advanced control strategies [12,13], such as preventive and corrective algorithms, allow to quickly monitor and adjust the system conditions, ensuring its stability.

Economic dispatch algorithms play a pivotal role in this process by optimizing the power set points of connected units while considering the forecast of loads and renewable generations. However, the straightforward application of these algorithms can push the μG to operate close to its stability limits, potentially compromising system security. Stability assessments and preventive strategies incorporating security margins are thus essential.

In the field of stability studies, several fundamental distinctions can be made, with the primary categorization occurring between static and dynamic analyses, both of which address the evaluation of voltage stability. Focusing specifically on static stability, it is crucial for networks integrating DERs to consider the specific types of generation adopted along with their control devices, and the locations within the grid where such resources are deployed [14–17]. Research involving comparative simulations [18,19] has applied different analytical frameworks, such as Jacobian matrices, voltage response sensitivity, and energy-based functions.

However, as μGs evolve toward increasingly complex architectures and the large-scale integration of non-dispatchable renewable energy

* Corresponding author.
E-mail address: g.amato1@phd.poliba.it (G. Amato).

https://doi.org/10.1016/j.ijepes.2025.111301
Received 21 January 2025; Received in revised form 25 July 2025; Accepted 18 October 2025
Available online 22 October 2025

sources intensifies, the scientific community's focus has progressively shifted beyond traditional analytical indicators. There is now a greater emphasis on control strategies capable not only of assessing but also proactively preventing unstable operating conditions. Within this context, model-based approaches such as Model Predictive Control (MPC) and robust optimization have garnered significant academic attention. Nonetheless, it is important to carefully consider their operational characteristics. MPC relies on a dynamic system model and requires solving a constrained optimization problem at each time step, which demands substantial computational resources and low computation times, requirements that are not always compatible with the hardware capabilities and real-time management constraints typical of μG [20]. Robust optimization, on the other hand, generates solutions that remain valid across all scenarios within a defined uncertainty set, but this often results in overly conservative planning. Consequently, the operating point tends to be shifted away from conditions of maximum economic efficiency even at the preventive stage [21]. Complementing these techniques, geometric methods have also been proposed for characterizing the secure operating region, including ellipsoidal domains. These provide a compact and computationally efficient representation suitable for contexts with limited computational availability and where a certain level of approximation is acceptable. However, the choice depends on the specific application, namely the network configuration and the available computational resources. When higher precision in defining the boundaries of the secure operating region is required, a more accurate characterization, such as that based on the convex hull, is preferable, as it enables a faithful representation of the stability boundary [22,23].

Among the various strategies proposed in the literature, the definition of a practical stability region described in [24] proves highly advantageous for implementing a practical control strategy in such systems. As this region is constructed offline for every possible network configuration, the high computational burden associated with it does not impact the real-time control. The strategy proposed in this work aims to restore insecure or unfeasible operating conditions, imposed by the system operator or the economic dispatch, within time frames compatible with the exigency of system management in the real-time. If the operating conditions provided at each time interval (e.g., every 15 min) are found to be either unfeasible or insufficiently secure, this practical and rapid method can identify a new operating condition that satisfies the desired security level while remaining close as much as possible to the initial economically optimal point and within typical operational management timescales.

In summary, the remainder of this paper is organized as follows. Section 2 provides a brief descriptive overview of the operating region of a μG, followed by an explanation of the proposed control strategy, supported by two-dimensional visual illustrations. In Section 3, the method is applied to a case study replicating a subset of the smart μG implemented in the PrInCE Lab of the Polytechnic University of Bari. Finally, Section 4 presents the conclusions drawn from the work and discusses potential future research directions in this field.

2. The control methodology

The Feasibility Region (FR) of a μG, as described in [24], is a Convex Hull (CH), a structure that encloses all feasible points within the system's operational hyperspace. Its construction minimizes the enclosed volume while avoiding the inclusion of infeasible points that could cause the under or overvoltage relays tripping, thus leading to a network blackout. This is ensured through the CH construction strategy, which is based on load flow analyses applied to operating conditions of the μG randomly generated with a standard normal distribution and the configuration of the protection relays installed within the network.

The geometric definition of the CH is established through *facets*, which are convex polygonal hypersurfaces that delineate the CH by connecting its vertices. The vertices represent the extreme points of the cloud of input operational conditions, while the *edges* define the boundaries of the facets.

Table 1
Assumed variability ranges for the generation of random μG operating points.

Rated power	Variability range	
A_n [kVA]	P [kW]	Q [kVAr]
60	[−60; 60]	[−60; 60]

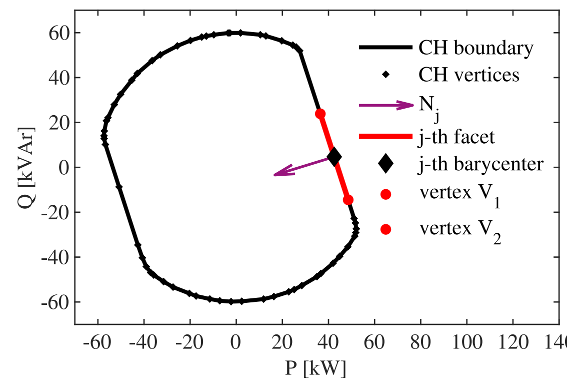

Fig. 1. Practical stability region of a single device, with geometric features associated with a representative facet.

In a two-dimensional space, the facets degenerate into line segments, as the CH itself becomes a polygon. For instance, applying the method described in [24] to a single network node with capability limits as outlined in Table 1 yields the two-dimensional CH depicted in Fig. 1. This CH consists of $N_F = 28$ facets and $N_V = 28$ vertices.

The data obtained from the implemented algorithm are instrumental in defining the normal vectors of each facet of the hull. These normal vectors are essential for the stability assessment phase of a generic operating condition $\mathbf{x}_p = [x_{p_1}; x_{p_2}; x_{p_3}; \dots; x_{p_n}]$, where each coordinate of the point corresponds to a controllable variable of a specific network node.

An operating point resulting from the economic dispatch algorithm is considered feasible if it lies within the constructed operational region. To achieve this result, it is necessary to compare, for each jth facet of the CH, the vector $\overline{\mathbf{V}}_j$ connecting its centroid to the operating point $\mathbf{x}_p$ and the vector pointing inside the region, $\overline{\mathbf{N}}_j$, normal to the facet. By iterating this comparison for all facets, we obtain the evidence of the position of $\mathbf{x}_p$ with regard to boundaries of the CH. The application of this approach to the previous 2-D example is shown in Fig. 2: in the case shown in the left side of the figure, the stability condition is satisfied, and the point lies within the feasible region; in the other case, the point is outside and, therefore, unstable.

However, it may occur that the economic dispatch algorithm results in an operating point $\mathbf{x}_p$ that satisfies the network's technical constraints, lies within the CH (i.e., is feasible), but is too close to its boundaries, thereby posing a risk to the secure operation of the μG. From a geometric perspective, this means that the minimum distance of the point from the CH boundary is less than a desired secure margin, denoted as sm.

2.1. Security assessment of an operating condition

Assuming that the economic dispatch algorithm provides the optimal economic solution to the 2-D problem, represented by the operating point $\mathbf{x}_p$ in Fig. 3, this point is certainly feasible, as it lies within the feasibility region, as confirmed by the stability assessment phase described in [24]. However, for $\mathbf{x}_p$ to be considered secure, in addition to being practically stable, it is necessary to verify that it maintains

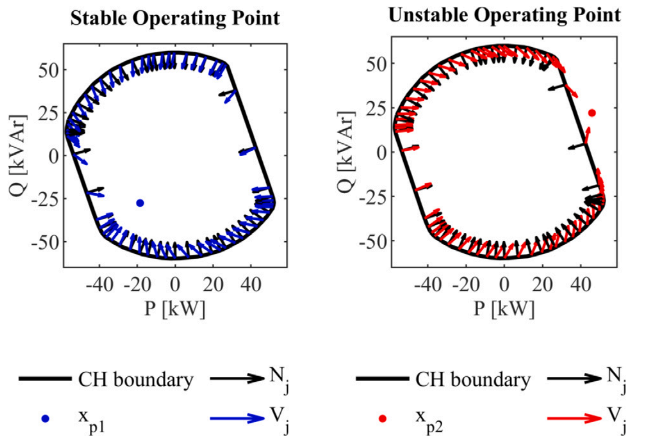

Fig. 2. Stability assessment of a generic working point via comparison between vectors $\overline{\mathbf{N}}_j$ and $\overline{\mathbf{V}}_j$.

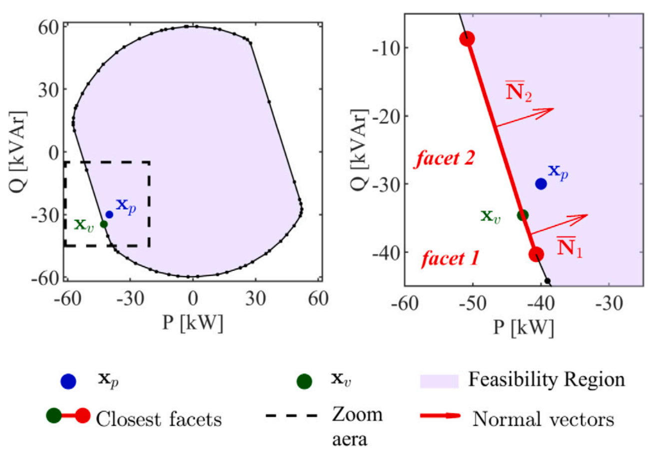

Fig. 3. Nearest vertex identification: in the zoomed view, facets sharing vertex $\mathbf{x}_v$ are highlighted in red, along with their normal vectors directed inward toward the feasible region.

a security margin *sm* from the boundary of the CH, which must be predetermined. Therefore, the first mandatory step of the proposed approach is to perform this verification.

As previously mentioned, the vertices of the structure are known from the construction of the feasibility region, and the normal vectors to each facet of the CH can be computed offline. To verify that the operating point $\mathbf{x}_p$ retains a distance from the boundary that is at least equal to the chosen security margin *sm*, the minimum distance of the point from the boundary of the stability region, i.e., from the closest facet of the structure, must be evaluated.

The minimum distance of a point from a facet is the one calculated along the line normal to the hypersurface passing through the point in question. Thus, it is appropriate to evaluate the distance from $\mathbf{x}_p$ to all facets, identify the smallest distance and comparing it to *sm*. It is important to note, however, that as the number of nodes in the μG increases, the size of the problem and the number N_F of facets in the structure also increases. Therefore, a practical and efficient method is needed to obtain the minimum distance of the point from the boundary, regardless of the size of the hyper-region in which it is contained. To speed up this procedure, the calculation is focused exclusively on the closest subset of facets to the given point.

The vertex $\mathbf{x}_v$ closest to $\mathbf{x}_p$ is selected from the list of N_V vertices of the CH by comparing the Euclidean distances between $\mathbf{x}_p$ and each

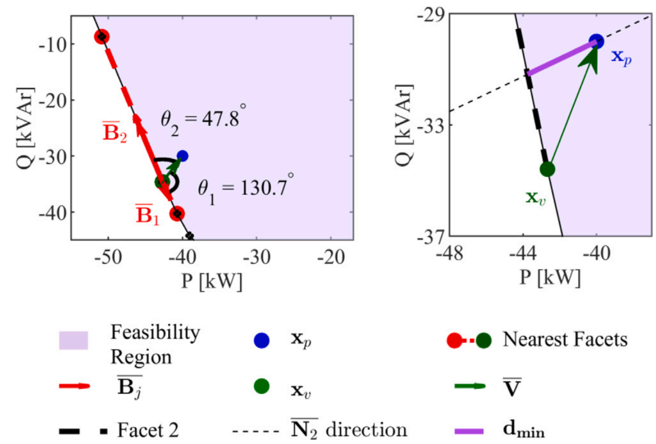

Fig. 4. Minimum distance computation: vectors $\overline{\mathbf{B}}_j$ and their angles θ_j with respect to vector $\overline{\mathbf{V}}$ are evaluated to identify the nearest facet; the minimum distance d_{min} is computed by projecting $\overline{\mathbf{V}}$ onto the normal of the nearest facet.

vertex $\mathbf{x}_{v_i}$, for $i = 1, \dots, N_V$, as defined in Eq. (1).

$$d_i = \sqrt{\mathbf{x}_{v_i}^2 - \mathbf{x}_p^2} \qquad for \quad i = 1, \dots, N_V \tag{1}$$

Among all computed distances d_i, the vertex $\mathbf{x}_v$ corresponding to the smallest distance is selected. Referring to the pilot example in this study, in Fig. 3, the vertex $\mathbf{x}_v$ identified as the closest in this analysis is marked in green.

From this information, it is possible to identify the n facets that share the vertex $\mathbf{x}_v$, corresponding to the subset of the closest facets being sought, indexed by $j = 1, \dots, n$. In Fig. 3, these facets and their corresponding normal vectors are highlighted in red. The identification of the hypersurface closest to $\mathbf{x}_p$ among those just identified is performed by comparing the projections of the vector $\overline{\mathbf{V}}$ connecting $\mathbf{x}_v$ to $\mathbf{x}_p$ onto each facet of the identified subset. To this end, the vector $\overline{\mathbf{B}}_j$ connecting $\mathbf{x}_v$ to the centroid of the jth facet of the identified subset (with $j = 1, \dots, n$) is determined.

In the example shown in Fig. 4, in which $j = \{1, 2\}$, the comparison is made between the projections of $\overline{\mathbf{V}}$ onto $\overline{\mathbf{B}}_1$ and $\overline{\mathbf{B}}_2$, calculated through the scalar products indicated in Eq. (2).

$$V_{B_j} = \overline{\mathbf{V}} \cdot \overline{\mathbf{B}}_j \qquad for \quad j = 1, 2 \tag{2}$$

The Eq. (2) will have a positive value if the angle θ_j between $\overline{\mathbf{V}}$ and $\overline{\mathbf{B}}_j$ satisfies Eq. (3), otherwise, it will be negative.

$$-90^\circ < \theta_j < 90^\circ \qquad for \quad j = 1, 2 \tag{3}$$

Referring to the pilot example in Fig. 4, it can be stated that:

- the angle θ_1 between $\overline{\mathbf{V}}$ and the vector $\overline{\mathbf{B}}_1$, which connects the vertex $\mathbf{x}_v$ to the centroid of the first facet, satisfies $90^\circ < \theta_1 = 130.7^\circ < 270^\circ$, and therefore $V_{B_1} < 0$;
- conversely, the angle θ_2 between $\overline{\mathbf{V}}$ and the vector $\overline{\mathbf{B}}_2$, which connects the vertex $\mathbf{x}_v$ to the centroid of the second facet, is $\theta_2 = 47.8^\circ < 90^\circ$, thus implying $V_{B_2} > 0$.

In the search for the closest facet, only the k facets that satisfy Eq. (4) are considered, while all others are discarded from the analysis.

$$V_{B_h} > 0 \qquad for \quad h = 1, \dots, k \tag{4}$$

In the case where all the projections just computed are negative or null, no hypersurface can be considered close to the point under examination. Therefore, the algorithm will select the direction along the vector $\overline{\mathbf{V}}$ as the preferred direction for movement. This means that

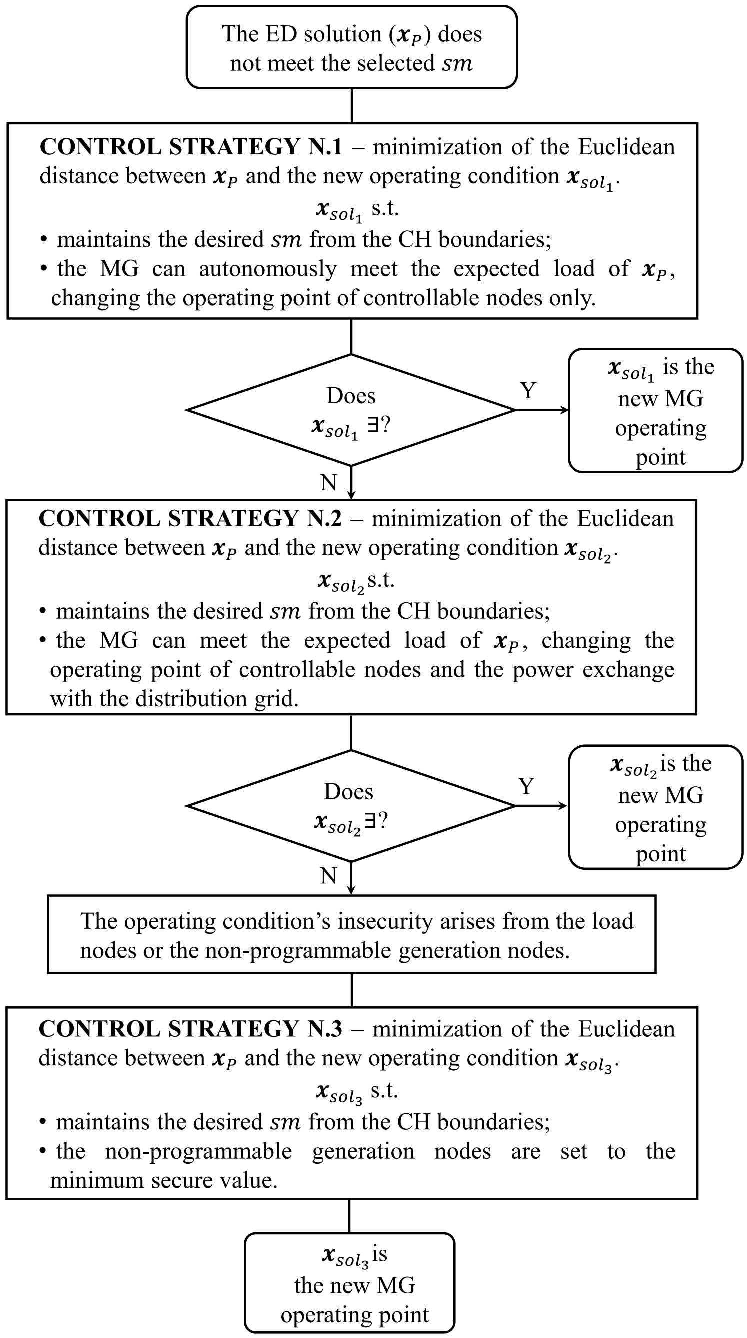

Fig. 5. Control strategy decision process.

the smallest distance from $\mathbf{x}_p$ to the boundary is exactly that between the point under test and the selected vertex $\mathbf{x}_v$.

The identification of the unique facet closest to the operational condition under examination considers the normal vectors $\overline{\mathbf{N}}_h$ (for $h = 1, \ldots, k$) to the k facets just identified. Following the same procedure as in the previous step, the projections of the vector $\overline{\mathbf{V}}$ onto each $\overline{\mathbf{N}}_h$ are calculated. This value will correspond to the distance from $\mathbf{x}_p$ to the hth facet. Therefore, the smallest value among these distances $\|\overline{\mathbf{V}}_{N_h}\|$ will correspond to the minimum distance of $\mathbf{x}_p$ from the boundary of the CH.

$$d_{min} = min\{V_{N_h} = \overline{\mathbf{V}} \cdot \overline{\mathbf{N}}_h \quad | \quad h = 1, \ldots, k\} \tag{5}$$

For the case under examination, only one facet satisfies Eq. (4), and thus the phase of searching for the closest facet simplifies to a single calculation, from which $d_{min} = V_{N_2}$ is obtained. To verify that $\mathbf{x}_p$ corresponds to a condition that is both secure and feasible, it will be sufficient to check that this distance is greater than or, at most, equal to the chosen sm as indicated in Eq. (6).

$$d_{min} \geq sm \tag{6}$$

If this condition is met, $\mathbf{x}_p$ can be sent to the network control system as the set point for the next time interval. Otherwise, it will be necessary to apply a preventive control strategy to bring the μG to operate in a different but feasible and secure condition $\mathbf{x}'_p$.

In this work, a very practical preventive control strategy is proposed. Through the solution of several optimization problems, the algorithm is able to achieve the desired results within time frames compatible with the online management of the system under examination. The flowchart representing the decision-making process studied in this work is shown in Fig. 5.

The three proposed control strategies are designed to operate sequentially and hierarchically, aiming to ensure system security while minimizing deviation from the economically optimal operating point. The process begins with Strategy N.1, which seeks to restore a secure condition by acting solely on controllable nodes, thus preserving full autonomy and maintaining proximity to the economic dispatch solution. If this approach proves insufficient, the algorithm advances to Strategy N.2, which leverages support from the external grid, providing additional flexibility but potentially increasing operational costs. Should this second strategy also be infeasible, Strategy N.3 is employed, involving more drastic corrective actions such as curtailment of non-dispatchable generation and load. This stepwise framework ensures that progressively more invasive and less economical interventions are implemented only when strictly necessary. It is important to acknowledge, however, that progressing from Strategy N.1 to N.3 entails a gradual departure from economic optimality in favor of preserving system security.

2.2. Control strategy N.1

Keep in mind that the aim is to identify a new operating point that satisfies the desired level of security and it is close as much as possible to the economically optimal operating point $\mathbf{x}_p$ provided by the economic dispatch algorithm, so as not to significantly alter the network configuration.

The ideal condition would be one where the new operational condition $\mathbf{x}'_p$ allows the μG to autonomously meet the load forecasted by $\mathbf{x}_p$, without altering the power exchange with the connected distribution network or reducing the generation output from non-dispatchable sources. In this regard, $\mathbf{x}'_p$ should satisfy the following characteristics:

- **a.** be feasible, that is, complying with the capability curves of the network devices and remaining within the region of practical stability;
- **b.** be secure, that is, maintaining a distance from the feasibility boundary at least equal to the selected margin sm;
- **c.** meet the load demand required by $\mathbf{x}_p$;
- **d.** maintain the power exchange equal to that of $\mathbf{x}_p$;
- **e.** ensure that the power generated by non-dispatchable sources remains as forecasted in $\mathbf{x}_p$;
- **f.** ensure that the necessary variation to minimize the distance between the two operational conditions occurs exclusively at controllable nodes.

Below are the basic elements of the optimization problem that need to be solved.

The *objective function* involves minimizing the Euclidean distance d between the sought solution $\mathbf{x}_{sol_1}$ and the initial condition $\mathbf{x}_p$:

$$\min_{\mathbf{x}_{\mathrm{sol}_1}} d(\mathbf{x}_{\mathrm{sol}_1};\mathbf{x}_p)^2 = \min_{\mathbf{x}_{\mathrm{sol}_1}}\Big((\mathbf{x}_{\mathrm{sol}_1}-\mathbf{x}_p)^T(\mathbf{x}_{\mathrm{sol}_1}-\mathbf{x}_p)\Big) \quad \textit{where} \quad \mathbf{x}_{\mathrm{sol}_1} = \left[x_{\mathrm{sol}_1,1}, x_{\mathrm{sol}_1,2}, \dots, x_{\mathrm{sol}_1,n}\right]^T \tag{7}$$

and n denotes the total number of optimization variables.

The *equality constraints* include maintaining the power at specific nodes. Let n_L represent the total number of loads, with P_{L_i} denoting the active power demand of load i, for $i = 1,\dots,n_L$. The condition ensuring load power invariance is:

$$\sum_{i=1}^{n_L}\left(P_{L_i}\right)_{\mathbf{x}_p} = \sum_{i=1}^{n_L}\left(P_{L_i}\right)_{\mathbf{x}_{\mathrm{sol}_1}} \tag{8}$$

Similarly, let n_{NPG} be the number of non-dispatchable (i.e., non-programmable) generation units, each supplying power P_{NPG_i}, for $i = 1,\dots,n_{\mathrm{NPG}}$. The related equality constraint is expressed as follows:

$$\sum_{i=1}^{n_{\mathrm{NPG}}}\left(P_{\mathrm{NPG}_i}\right)_{\mathbf{x}_p} = \sum_{i=1}^{n_{\mathrm{NPG}}}\left(P_{\mathrm{NPG}_i}\right)_{\mathbf{x}_{\mathrm{sol}_1}} \tag{9}$$

Finally, considering n total nodes, where P_{CG_i} and P_{NPG_i} represent the controllable and non-programmable generation at node i, and P_{L_i} the load demand at node i, the net power exchanged with the grid is conserved as:

$$\sum_{i=1}^{n}\Big(P_{\mathrm{CG}_i}+P_{\mathrm{NPG}_i}-P_{L_i}\Big)_{\mathbf{x}_p} = \sum_{i=1}^{n}\Big(P_{\mathrm{CG}_i}+P_{\mathrm{NPG}_i}-P_{L_i}\Big)_{\mathbf{x}_{\mathrm{sol}_1}} \tag{10}$$

which ensures compliance with constraints **c**, **d**, **e**, and **f**.

The *inequality constraints*, on the other hand, are divided into two categories. The first group concerns technical constraints on controllable nodes: the power in operation must satisfy the capability constraints (i.e. active power P, reactive power Q and apparent power A) of the associated devices according to the requirement **a**. Therefore, for each ith controllable device, with $i = 1,\dots,n_{CG}$, the following inequalities must be satisfied:

$$P^i_{min} \le P^i_{\mathbf{x}_{\mathrm{sol}_1}} \le P^i_{max} \tag{11}$$

$$Q^i_{min} \le Q^i_{\mathbf{x}_{\mathrm{sol}_1}} \le Q^i_{max} \tag{12}$$

$$0 \le \left(P^i_{\mathbf{x}_{\mathrm{sol}_1}}\right)^2 + \left(Q^i_{\mathbf{x}_{\mathrm{sol}_1}}\right)^2 \le \left(A^i_{max}\right)^2 \tag{13}$$

The second group of inequality constraints accounts for the geometric positioning of the operating point within the hyperspace. Following the stability assessment framework outlined in [24], let $\overline{\mathbf{N}}_j$ denote the unit normal vector to the jth facet of the CH, and let $\overline{\mathbf{V}}_{j-\mathbf{x}_{\mathrm{sol}_1}}$ represent the vector from the centroid of that facet to the operating point $\mathbf{x}_{\mathrm{sol}_1}$. To ensure that the operating point lies within the CH (and is thus feasible with respect to requirement **a**) the scalar quantity $c_{jp_{\mathrm{sol}}}$, that quantifies the signed projection of the vector $\overline{\mathbf{V}}_{j-\mathbf{x}_{\mathrm{sol}_1}}$ onto $\overline{\mathbf{N}}_j$, must satisfy the inequality in Eq. (14). Simultaneously, it is necessary to check Eq. (6) to ensure the desired sm according to the requirement **b**.

$$c_{jp_{sol}} = \overline{\mathbf{N}}_j \cdot \overline{\mathbf{V}}_{j-\mathbf{x}_{\mathrm{sol}_1}} \ge 0 \qquad \forall j = 1,\dots,N_F \tag{14}$$

The most desirable solution, $\mathbf{x}_{\mathrm{sol}_1}$, if it exists, would be sent as the set-point $\mathbf{x}'_p = \mathbf{x}_{\mathrm{sol}_1}$ to the μG. Therefore, μG would operate in a practically feasible, stable, and secure condition, very close to the economically optimal one. However, this problem may not converge to a solution. In such a case, the proposed algorithm would proceed to the second control strategy.

2.3. Control strategy N.2

If the most desirable solution cannot be autonomously achieved by the μG, considering an operational configuration of the μG in parallel with the distribution network, the second control strategy involves support from the external grid. Therefore, the objective of this optimization problem is to find $\mathbf{x}_{\mathrm{sol}_2}$ such that it satisfies all the previous requirements, except for **d** (i.e., Eq. (10)). The optimization problem representing this control strategy, therefore, will have the overall mathematical formulation as in Eq. (15), where the indices used are $\forall i = 1,\dots,n_{\mathrm{CG}}$ and $\forall j = 1,\dots,N_F$.

$$\min_{\mathbf{x}_{\mathrm{sol}_2}} d(\mathbf{x}_{\mathrm{sol}_2};\mathbf{x}_p)^2 = \min_{\mathbf{x}_{\mathrm{sol}_2}}\Big((\mathbf{x}_{\mathrm{sol}_2}-\mathbf{x}_p)^T(\mathbf{x}_{\mathrm{sol}_2}-\mathbf{x}_p)\Big)$$
$$s.t.\ \begin{cases} \sum_{i=1}^{n_L}(P_{L_i})_{\mathbf{x}_p} = \sum_{i=1}^{n_L}(P_{L_i})_{\mathbf{x}_{\mathrm{sol}_2}} \\ \sum_{i=1}^{n_{\mathrm{NPG}}}(P_{\mathrm{NPG}_i})_{\mathbf{x}_p} = \sum_{i=1}^{n_{\mathrm{NPG}}}(P_{\mathrm{NPG}_i})_{\mathbf{x}_{\mathrm{sol}_2}} \\ P^i_{\min} \le P^i_{\mathbf{x}_{\mathrm{sol}_2}} \le P^i_{\max} \\ Q^i_{\min} \le Q^i_{\mathbf{x}_{\mathrm{sol}_2}} \le Q^i_{\max} \\ 0 \le (P^i_{\mathbf{x}_{\mathrm{sol}_2}})^2 + (Q^i_{\mathbf{x}_{\mathrm{sol}_2}})^2 \le (A^i_{\max})^2 \\ c_{jp_{\mathrm{sol}_2}} = \overline{\mathbf{N}}_j \cdot \overline{\mathbf{V}}_{j-\mathbf{x}_{\mathrm{sol}_2}} \ge 0 \\ d_{\min} \ge sm \end{cases} \tag{15}$$

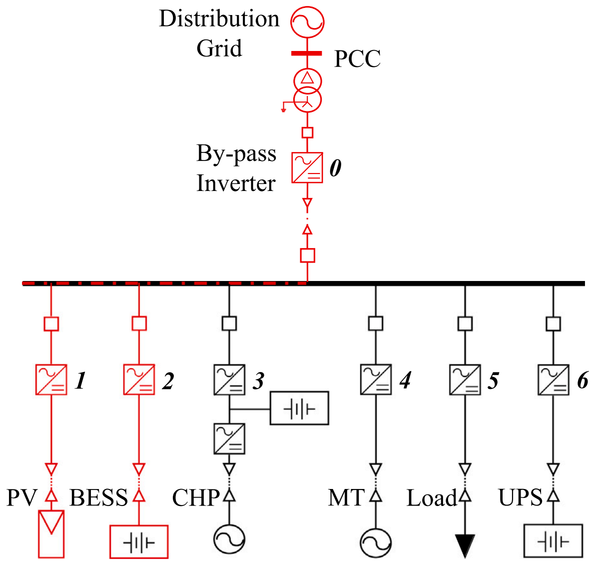

Fig. 6. PrInCE Lab μG layout.

If $\mathbf{x}_{\mathrm{sol}_2}$ exists, it will be the new operating condition $\mathbf{x}'_p$ to be sent to the μG control system. Although this solution may depart from the economically optimal configuration due to the altered power exchange with the distribution grid, it nonetheless represents a technically robust and strategically justified outcome. The adopted formulation prioritizes the stable and secure operation of the μG, representing a rigorous and well-balanced compromise that ensures system reliability while preserving an acceptable alignment with economic performance. Since the new solution is constructed to be geometrically as close as possible to the economically optimal one, the resulting power setpoints will deviate only marginally from those corresponding to the minimum cost, thereby ensuring a near-invariance of economic efficiency. However, it may still happen that the problem does not converge even in this case, forcing the algorithm to proceed to the last control strategy.

2.4. Control strategy N.3

If none of the previously outlined strategies produce a feasible solution, a more substantial corrective intervention is required. This situation typically occurs when prior optimization attempts fail due to instability issues associated with non-controllable nodes or load demand. In such cases, the only effective course of action involves systematically reducing the output of non-dispatchable generation units and, if necessary, curtailing load demand. These adjustments arise naturally from the optimization framework itself, representing the unique configuration that satisfies all stability and security constraints without relying on predefined curtailment policies.

Such modifications apply across all nodes, including non-dispatchable sources and loads, to restore the operating point within the permissible boundaries defined by the stability region's geometric constraints. Consequently, the relevant system equations, Eqs. (7) and (8), are updated in accordance with the constraints specified in Eqs. (16) and (17), while controllable nodes maintain full flexibility to modulate their output as needed.

Although economic optimization is not explicitly incorporated at this stage, the resulting operating point $\mathbf{x}_{\mathrm{sol}_3}$ ensures a secure and stable μG configuration. This outcome may involve some underutilization of renewable energy resources and load curtailment, but such trade-offs are consciously accepted to prioritize the fundamental goal of system stability. This approach guarantees the reliable and continuous operation of the μG under a range of conditions, consistent with the

Table 2
Assumed variability ranges for the generation of the random MG operating points.

Bus id	Rated power	Variability range	
	A_n [kVA]	P [kW]	Q [kVAr]
1	50	[0; 50]	–
2	60	[−60; 60]	[−60; 60]

preventive nature of this control phase. Thus, the optimization problem representing this strategy is summarized as in Eq. (18).

Through this practical preventive control method, the operating point provided by the economic dispatch algorithm that does not meet the desired security level will be modified within a time frame compatible with the traditional management of the electrical system. In fact, within the quarter-hour required for the system to provide the subsequent operating condition, it will be possible to verify its practical stability and, if necessary, find a new operating point that aligns with the security level chosen by the operator.

$$\sum_{i=1}^{n_L}(P_{L_i})_{\mathbf{x}_p} > \sum_{i=1}^{n_L}(P_{L_i})_{\mathbf{x}_{\mathrm{sol}_3}} \tag{16}$$

$$\sum_{i=1}^{n_L}(P_{L_i})_{\mathbf{x}_p} > \sum_{i=1}^{n_L}(P_{L_i})_{\mathbf{x}_{\mathrm{sol}_3}} \tag{17}$$

$$\min_{\mathbf{x}_{\mathrm{sol}_3}} d(\mathbf{x}_{\mathrm{sol}_3};\mathbf{x}_p)^2 = \min_{\mathbf{x}_{\mathrm{sol}_3}}\left((\mathbf{x}_{\mathrm{sol}_3}-\mathbf{x}_p)^T(\mathbf{x}_{\mathrm{sol}_3}-\mathbf{x}_p)\right)$$
$$s.t.\ \begin{cases} \sum_{i=1}^{n_L}(P_{L_i})_{\mathbf{x}_p} > \sum_{i=1}^{n_L}(P_{L_i})_{\mathbf{x}_{\mathrm{sol}_3}} \\ \sum_{i=1}^{n_{\mathrm{NPG}}}(P_{\mathrm{NPG}_i})_{\mathbf{x}_p} > \sum_{i=1}^{n_{\mathrm{NPG}}}(P_{\mathrm{NPG}_i})_{\mathbf{x}_{\mathrm{sol}_3}} \\ P^i_{\min} \le P^i_{\mathbf{x}_{\mathrm{sol}_3}} \le P^i_{\max} \\ Q^i_{\min} \le Q^i_{\mathbf{x}_{\mathrm{sol}_3}} \le Q^i_{\max} \\ 0 \le (P^i_{\mathbf{x}_{\mathrm{sol}_3}})^2 + (Q^i_{\mathbf{x}_{\mathrm{sol}_3}})^2 \le (A^i_{\max})^2 \\ c_{jp_{\mathrm{sol}_3}} = \overline{\mathbf{N}}_j \cdot \overline{\mathbf{V}}_{j-\mathbf{x}_{\mathrm{sol}_3}} \ge 0 \\ d_{\min} \ge sm \end{cases} \tag{18}$$

3. Case study: The PrInCE μG

The method described above has been tested on the static model of the μG installed at the PrInCE Lab of the Polytechnic University of Bari, whose complete layout is shown in Fig. 6. The μG has a radial configuration and it consists of 7 nodes and 6 lines, but for convenience of representation, the subset highlighted in red in the figure is referenced here. This allows for the derivation of a 3-D graphical representation useful for demonstrating the validity of the proposed method.

The capability curves of the devices considered in the analysis are those shown in Table 2 and allow for the determination of the feasibility region corresponding to the considered subset, similar to the one identified in [24].

At this point, it is assumed that the economic dispatch algorithm provides the optimal solution $\mathbf{x}_p$, represented in red in Fig. 7.

This is certainly feasible from a technical standpoint, as it lies within the identified CH, but to be considered a secure operating condition, it must be verified that it maintains a distance from the perimeter of the structure at least equal to the desired sm. Starting from the identification of the vertex closest to the point of interest, the vertex $\mathbf{x}_v$ is selected, and the hyperplanes associated with it, shown in green in Fig. 7, are identified. Among these, the hypersurface closest to the point $\mathbf{x}_p$ is determined by applying the procedure described in Section 2.1, whose graphical representation is provided in Fig. 8. Specifically, among the $n = 10$ facets initially selected as the nearest

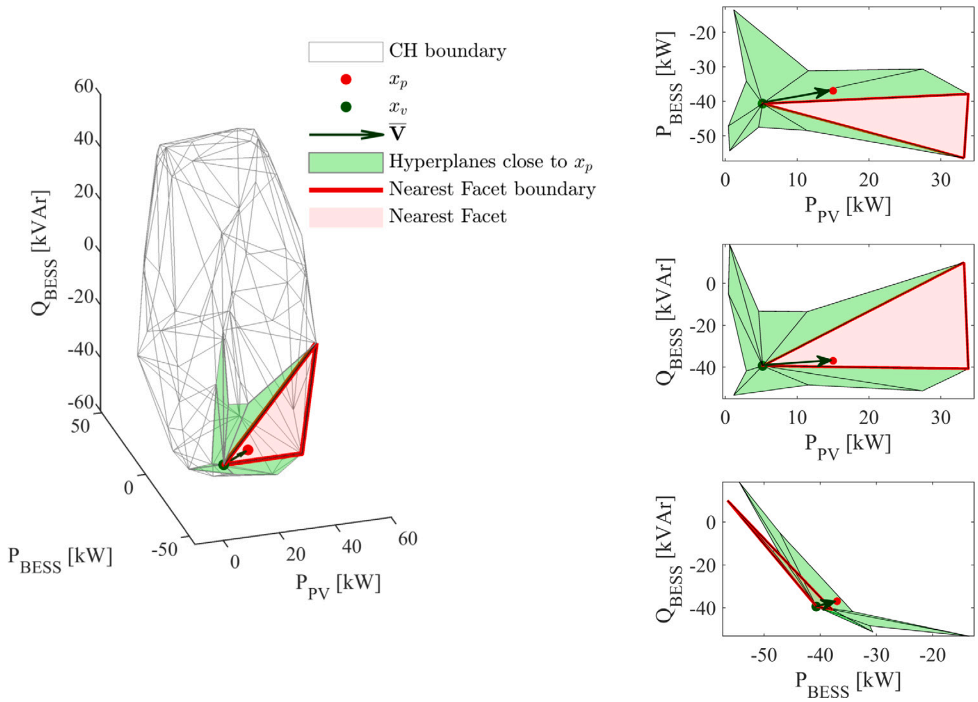

Fig. 7. Identification of the facet closest to $\mathbf{x}_p$ and its projection onto the main planes.

to the point $\mathbf{x}_p$, the one highlighted in red is identified as the facet for which the projection of the vector $\overline{\mathbf{V}}$ along the direction of vector normal to the hypersurface (Fig. 8a) satisfies the condition expressed in Eq. (5). The comparison between the computed minimum distance d_{min} and the assigned security margin sm (equal to 10 kVA in this pilot example) clearly shows, as illustrated in Fig. 8b, that $d_{min} < sm$. To bring the μG to operate in a secure condition, the control strategy proposed in Section 2 is applied.

As indicated in Section 2.2, the desired solution is the one that, while being close to that provided by the economic dispatch, allows the μG to autonomously meet its load by simply re-dispatching its controllable units.

Therefore, the optimization problem becomes the one outlined in Eq. (19), where $\mathbf{x}_{\text{sol}_1} = [x_{\text{sol}_{1,P_{PV}}},\ x_{\text{sol}_{1,P_{BESS}}},\ x_{\text{sol}_{1,Q_{BESS}}}]^T$, and the capability limits are those expressed in Table 2.

$$\min_{\mathbf{x}_{\text{sol}_1}} d(\mathbf{x}_{\text{sol}_1};\mathbf{x}_p)^2 = \min_{\mathbf{x}_{\text{sol}_1}}\Big((\mathbf{x}_{\text{sol}_1}-\mathbf{x}_p)^T(\mathbf{x}_{\text{sol}_1}-\mathbf{x}_p)\Big)$$
$$s.t.\ \begin{cases} P^{PV}_{\mathbf{x}_p} = P^{PV}_{\mathbf{x}_{\text{sol}_1}} \\ P^{PV}_{\mathbf{x}_p} + P^{BESS}_{\mathbf{x}_p} = P^{PV}_{\mathbf{x}_{\text{sol}_1}} + P^{BESS}_{\mathbf{x}_{\text{sol}_1}} \\ Q^{BESS}_{\mathbf{x}_p} = Q^{BESS}_{\mathbf{x}_{\text{sol}_1}} \\ P^{PV}_{min} \le P^{PV}_{\mathbf{x}_{\text{sol}_1}} \le P^{PV}_{max} \\ P^{BESS}_{min} \le P^{BESS}_{\mathbf{x}_{\text{sol}_1}} \le P^{BESS}_{max} \\ Q^{BESS}_{min} \le Q^{BESS}_{\mathbf{x}_{\text{sol}_1}} \le Q^{BESS}_{max} \\ 0 \le (P^{BESS}_{\mathbf{x}_{\text{sol}_1}})^2 + (Q^{BESS}_{\mathbf{x}_{\text{sol}_1}})^2 \le (A^{BESS}_{max})^2 \\ c_{jp_{\text{sol}_1}} = \overline{\mathbf{N}}_j \cdot \overline{\mathbf{V}}_{j-\mathbf{x}_{\text{sol}_1}} \ge 0 \quad \forall j = 1\ldots, N_F \\ d_{\min} \ge sm \end{cases} \tag{19}$$

From the constraints of this problem, it is evident that, in this specific case, the only variable allowed to move in the hyperspace is $P^{BESS}_{\mathbf{x}_{\text{sol}_1}}$, but, due to the requirement to satisfy the second equality constraint, it will remain constant. Therefore, the optimization problem associated with this first step will not converge.

The second optimization problem aims to search for the optimal rescheduling solution for the internal units of the μG without altering the power exchange, but potentially reducing the power of non-dispatchable generation units or the load. In this specific case, it is noted that the solution that would satisfy the technical constraints would involve a reduction in power values, but this would lead to further approaching the operating condition to the stability boundary. Therefore, this optimization problem also does not converge.

$$\min_{\mathbf{x}_{\text{sol}_2}} d(\mathbf{x}_{\text{sol}_2};\mathbf{x}_p)^2 = \min_{\mathbf{x}_{\text{sol}_2}}\Big((\mathbf{x}_{\text{sol}_2}-\mathbf{x}_p)^T(\mathbf{x}_{\text{sol}_2}-\mathbf{x}_p)\Big)$$
$$s.t.\ \begin{cases} P^{PV}_{\mathbf{x}_p} \ge P^{PV}_{\mathbf{x}_{\text{sol}_2}} \\ P^{PV}_{\mathbf{x}_p} + P^{BESS}_{\mathbf{x}_p} \ge P^{PV}_{\mathbf{x}_{\text{sol}_2}} + P^{BESS}_{\mathbf{x}_{\text{sol}_2}} \\ Q^{BESS}_{\mathbf{x}_p} \ge Q^{BESS}_{\mathbf{x}_{\text{sol}_2}} \\ P^{PV}_{min} \le P^{PV}_{\mathbf{x}_{\text{sol}_2}} \le P^{PV}_{max} \\ P^{BESS}_{min} \le P^{BESS}_{\mathbf{x}_{\text{sol}_2}} \le P^{BESS}_{max} \\ Q^{BESS}_{min} \le Q^{BESS}_{\mathbf{x}_{\text{sol}_2}} \le Q^{BESS}_{max} \\ 0 \le (P^{BESS}_{\mathbf{x}_{\text{sol}_2}})^2 + (Q^{BESS}_{\mathbf{x}_{\text{sol}_2}})^2 \le (A^{BESS}_{max})^2 \\ c_{jp_{\text{sol}_2}} = \overline{\mathbf{N}}_j \cdot \overline{\mathbf{V}}_{j-\mathbf{x}_{\text{sol}_2}} \ge 0 \quad \forall j = 1\ldots, N_F \\ d_{\min} \ge sm \end{cases} \tag{20}$$

At this point, the only feasible solution is to bring the μG to operate securely by adjusting the power flow exchange with the distribution grid, solving Eq. (20). The optimal solution $\mathbf{x}'_p$ is shown in blue in Fig. 8.

The security assessment of the operating point provided by the economic dispatch, along with the potential application of corrective actions, entails a computational burden that varies depending on whether the point already satisfies the predefined security margin and on the step at which convergence is achieved, either at the first control iteration or at the last. To offer a quantitative benchmark, 15000 plausible operating points, representative of typical behavior of the

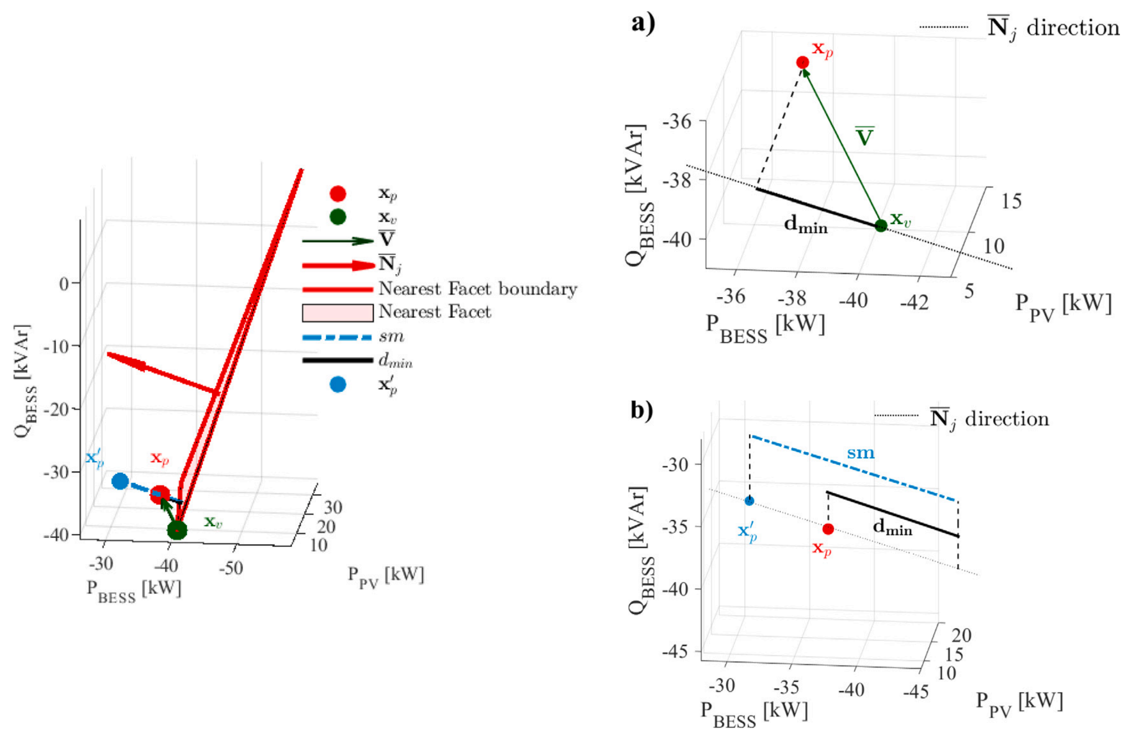

Fig. 8. Distance evaluation between $\mathbf{x}_p$ and the CH boundary. **(a)** Projection of $\overline{\mathbf{V}}$ onto the direction of $\overline{\mathbf{N}_j}$ to compute d_{min}. **(b)** Comparison between d_{min} and sm to determine the updated point $\mathbf{x}'_\mathbf{p}$.

system in Fig. 6, were randomly selected. The computational times required by the preventive control phase for this dataset are reported in Table 3. It is worth noting that, for all operating points in the dataset, the total time required for both the security assessment and the associated control phase remains significantly under the typical computational budget allocated for real-time μG operation, which is commonly set to a 15 min interval. Table 4 summarizes the power deviations between the original operating points and the resulting points after corrective actions, as well as the total computation times required for both the security assessment and the control phases. The comparison includes three methods: the geometric approach proposed in this work (CH), the method based on the Minimum Volume Enclosing Ellipsoid (MVEE, [22]), and the widely adopted Continuation Power Flow (CPF, [25]). Each of these methods has demonstrated effectiveness in restoring secure operating conditions. CPF is a well-established and robust technique, particularly appreciated for its ability to trace system trajectories close to voltage collapse points. In the considered test case, however, CPF applied a uniform power adjustment across all nodes, including those not directly involved in the security constraint violation. This led to unnecessary curtailment of photovoltaic generation, with a resulting increase in operating costs. CPF also required higher computation times compared to the proposed approach. The MVEE-based method offers a favorable trade-off between accuracy and speed. Its ellipsoidal representation provides a compact and computationally efficient estimate of the stability region. Nevertheless, due to the regularity of the ellipsoidal shape, the approximation may be conservative, leading to control actions that slightly deviate from the economically optimal operating point identified by the dispatch algorithm. The proposed CH-based method combines the flexibility of a geometric representation with high computational efficiency. It achieves a more accurate approximation of the feasible region, enabling localized corrective actions that preserve system security while remaining close to the optimal economic solution. The results confirm the suitability of this method as a practical and scalable solution for preventive security assessment in modern μGs operation.

The effectiveness of the proposed method is further supported by the findings in [23], which demonstrate that the convex hull-based control strategy achieves markedly higher accuracy than conventional geometric approaches. In particular, it enables the system to operate within tighter security margins, thereby enhancing overall system robustness and efficiency. While the computational effort increases with the complexity of the network, it is primarily the number of facets defining the feasibility region that drives the cost and the corresponding number of normal vectors involved with scalar products. However, the most significant computational effort is concentrated in the offline construction of the feasibility region, which does not affect the method's real-time efficiency. During this preliminary phase, all feasible regions and their associated normal vectors are computed once and stored, enabling fast and flexible access during μG operation. The framework features a modular architecture that allows seamless adaptation to changes in network topology or operational constraints without requiring a full recomputation of the feasibility set. When the system configuration or equipment limits change, the appropriate region can be directly retrieved from the precomputed archive, using real-time measurements solely to identify the most suitable parameter set. This eliminates the need to relaunch the offline procedure and ensures uninterrupted operation.

4. Conclusion and future works

This paper proposes a fast and efficient preventive control strategy to ensure the secure operation of a μG. Starting from the definition of a stability hyper-region as described in [24], an operating point provided by the system's economic dispatch that does not meet the desired security level is modified. At the end of the time interval required for managing the system, the μG is brought to operate in a new feasible and secure operating condition. The proposed approach, based on analytical expressions and geometric studies, is applicable regardless of the number of devices comprising the overall system. Certainly, the offline phase of building the hyper-region representing the feasible operation of the μG will incur a computational burden proportional to

Table 3
Execution times for the preventive control strategy applied to 15000 operating points.

Total time	Average time per point	Minimum time per point	Maximum time per point
12′ 58″	0.067″	1.5e−4′	1′ 22′

Table 4
Comparison of power deviations and computation times among three different preventive control methods: CH, MVEE, and CPF.

Method	Power deviation	Computational burden
CH	3.37 [kVA]	1.03 [s]
MVEE	5.96 [kVA]	2.04 [s]
CPF	5.98 [kVA]	2.86 [s]

the size of the problem. Meanwhile, the preventive control phase of the system's operating condition will always be compatible with the standard operating times of a μG.

The choice to adopt a limited subset of the experimental μG in the PrInCE Lab as a case study was driven by the desire to provide the reader with a visual (two-dimensional or, at most, three-dimensional) representation of the method. However, this choice does not preclude the possibility of extending the analysis to the entire system and achieving robust results even without direct visualization.

From a forward-looking perspective, this study opens up a range of promising directions for further development. One particularly fertile area involves the integration of machine learning and artificial intelligence tools, which could provide the system with adaptive capabilities and enable real-time control decisions in the presence of uncertainty and evolving operational conditions. These tools could complement the analytical core of the method by learning from historical data, identifying patterns in system behavior, and refining the estimation of feasible and secure regions over time. Another dimension worth exploring involves the potential role of distributed ledger technologies, such as blockchain, which could strengthen the transparency, auditability, and decentralized coordination of preventive control actions in distributed energy environments. In addition to these technological advancements, future work should address the refinement of strategies for managing non-controllable nodes. In the present formulation, reductions in power output or load demand at these nodes are applied without explicit prioritization or economic optimization, stemming instead from the geometric constraints imposed by the stability region. Although this approach ensures a secure and stable operating point, it may lead to suboptimal utilization of renewable resources and load curtailment. This trade-off is intentional, reflecting the primary objective of safeguarding μG security. Nonetheless, the framework is designed to accommodate more advanced control policies that integrate economic trade-offs and prioritization criteria, which can be implemented in future work to improve operational efficiency without compromising system security. Moreover, extending the methodology to accommodate a broader set of μG configurations, including both islanded and grid-connected modes, will be essential to assess its robustness and generalizability across different deployment contexts. This naturally entails addressing the associated computational and implementation challenges, especially in systems characterized by high dimensionality, strong coupling among devices, and time-sensitive operational requirements. Finally, hybrid approaches that synergistically combine model-based formulations with data-driven enhancements may offer an optimal balance between interpretability, performance, and scalability. Such advancements would not only enrich the theoretical underpinnings of preventive control in power systems but also accelerate its transition from concept to practice, ultimately contributing to the development of next-generation energy systems that are secure, resilient, and economically efficient.

CRediT authorship contribution statement

Giulia Amato: Writing – original draft, Validation, Software, Methodology, Formal analysis, Data curation. **Luigi Pio Savastio:** Visualization, Investigation. **Enrico Elio De Tuglie:** Writing – review & editing, Supervision, Resources, Project administration, Funding acquisition, Conceptualization.

Declaration of competing interest

The authors declare that they have no known competing financial interests or personal relationships that could have appeared to influence the work reported in this paper.

Acknowledgments

This study was carried out within the NEST - Network 4 Energy Sustainable Transition (D.D. 1243 02/08/2022, PE00000021). This work was supported by National Recovery and Resilience Plan (NRRP), Italy, Mission 4 Component 2 Investment 1.3, funded from the European Union – NextGenerationEU. This manuscript reflects only the authors' views and opinions, neither the European Union nor the European Commission can be considered responsible for them.

Data availability

The data that has been used is confidential.

References

[1] Kennedy J, Trewin B, Betts R, Thorne P, Foster P, Siegmund P, Ziese M, Mishra S, Uhlenbrook S, Alvar-Beltran J, Gialletti A. State of the climate 2024. 2024, Update for COP29.
[2] Ahmed F, Kez DAl, McLoone S, Best RJ, Cameron C, Foley A. Dynamic grid stability in low carbon power systems with minimum inertia. Renew Energy 2023;210:486–506.
[3] Makolo P, Zamora R, Lie TT. The role of inertia for grid flexibility under high penetration of variable renewables-a review of challenges and solutions. Renew Sustain Energy Rev 2021;147:111223.
[4] Li S, Voigt A, Schäfer AI, Richards BS. Renewable energy powered membrane technology: Energy buffering control system for improved resilience to periodic fluctuations of solar irradiance. Renew Energy 2020;149:877–89.
[5] Shair J, Li H, Hu J, Xie X. Power system stability issues, classifications and research prospects in the context of high-penetration of renewables and power electronics. Renew Sustain Energy Rev 2021;145:111111.
[6] Swapna V, Gayatri MTL. Power quality issues of grid integration of distributed generation: A review. In: 2021 international conference on computational performance evaluation (comPE). IEEE.; 2021, p. 142–7.
[7] Li MJ, Chi KT. Identification of nodes most vulnerable to voltage collapse in cascading failures of power systems. In: 2023 IEEE international symposium on circuits and systems, vol. 1–5, IEEE; 2023.
[8] Wang C, Yan J, Marnay C, Djilali N, Dahlquist E, Wu J, Jia H. Distributed energy and microgrids (DEM). Appl Energy 2018;210:685–9.
[9] Garcia-Torres F, Bordons C, Tobajas J, Real-Calvo R, Santiago I, Grieu S. Stochastic optimization of microgrids with hybrid energy storage systems for grid flexibility services considering energy forecast uncertainties. IEEE Trans Power Syst 2021;36(6):5537–47.
[10] Ghosh P, De M. Impact of microgrid towards power system resilience improvement during extreme events. In: 2021 international conference on computational performance evaluation, vol. 767–772, IEEE; 2021.
[11] Stasinos EIE, Trakas DN, Hatziargyriou ND. Microgrids for power system resilience enhancement. Ienergy 2022;1(2):158–69.

[12] Mohammadi F, Mohammadi-Ivatloo B, Gharehpetian GB, Ali MH, Wei W, Erdinç O, Shirkhani M. Robust control strategies for microgrids: A review. IEEE Syst J 2022;16(2):2401–12.
[13] Li ZL, Li P, Yuan ZP, Xia J, Tian D. Optimized utilization of distributed renewable energies for island microgrid clusters considering solar-wind correlation. Electr Power Syst Res 2022;206:107822.
[14] Rahman S, Saha S, Islam SN, Arif MT, Mosadeghy M, Haque ME, Oo AM. Analysis of power grid voltage stability with high penetration of solar PV systems. IEEE Trans Ind Appl 2021;57(3):2245–57.
[15] Aziz T, Dahal S, Mithulananthan N, Saha TK. Impact of widespread penetrations of renewable generation on distribution system stability. In: International conference on electrical & computer engineering, vol. 338–341, IEEE; 2010.
[16] Jhala K, Natarajan B, Pahwa A. Probabilistic voltage sensitivity analysis (PVSA) for random spatial distribution of active consumers. In: 2018 IEEE power & energy society innovative smart grid technologies conference, vol. 1–5, IEEE; 2018.
[17] Jhala K, Krishnan V, Natarajan B, Zhang Y. Data-driven preemptive voltage monitoring and control using probabilistic voltage sensitivities. In: 2019 IEEE power & energy society general meeting, vol. 1–5, IEEE; 2019.
[18] Moon YH, Ryu HS, Lee JG, Kim B. Uniqueness of static voltage stability analysis in power systems. In: 2001 power engineering society summer meeting. conference proceedings (cat. no. 01CH37262), vol. 3, IEEE.; 2001, p. 1536–41.
[19] Lou Y, Ou Z, Tong Z, Tang W, Li Z, Yang K. Static volatge stability evaluation on the urban power system by continuation power flow. In 2022 5th international conference on energy. In: Electrical and power engineering. IEEE; 2022, p. 833–8.
[20] Garcia-Torres F, Zafra-Cabeza A, Silva C, Grieu S, Darure T, Estanqueiro A. Model predictive control for microgrid functionalities: Review and future challenges. Energies 2021;14(5):1296.
[21] Yang J, Su C. Robust optimization of microgrid based on renewable distributed power generation and load demand uncertainty. Energy 2021;223:120043.
[22] Amato G, De Tuglie EE, Martella A, Montegiglio P, Rasolomampionona D, Pai HY. A method for Practical Stability Region evaluation and a preventive control strategy for MicroGrids. IEEE Trans Ind Appl 2025.
[23] Amato G, Savastio LP, Maulà G, De Tuglie EE. Practical static stability assessment for smart MicroGrids: a comparison between the MVEE and the convex hull. In: 2024 IEEE international humanitarian technologies conference, vol. 1–6, IEEE.; 2024.
[24] Amato G, De Tuglie EE, Montegiglio P. Geometrical method for a fast practical static stability region evaluation of a smart microgrid. Sustain Energy, Grids Netw 2024;38:101387.
[25] Lou Y, Ou Z, Tong Z, Tang W, Li Z, Yang K. Static volatge stability evaluation on the urban power system by continuation power flow. In: 2022 5th international conference on energy, electrical and power engineering, vol. 833–838, IEEE; 2022.